Optimization of Cascaded Control Gains of Grid-Forming Based Energy Conversion System

Taoufik Qoria
Seif Eddine Ben Haoua
Raul Santiago Munoz Aguilar
Embedded Systems Department EAE
Machinenfabrik Reinhausen
Regensburg, Germany
{t.qoria}@reinhausen.com

Hicham Fakham
Xavier Guillaud
Univ. Lille, Arts et Metiers Institute of Technology,
Centrale Lille, Yncrea Hauts-de-France, ULR 2697, L2EP,
Lille, France

***Abstract*—This paper proposes an optimal tuning of the inner cascaded control gains in the grid-forming configuration. The study delves into the intricacies of the system, presenting a comprehensive mathematical model that describes both the plant and the control. The significance of the optimization algorithm in the tuning of the control gains is highlighted compared to the conventional methods. In high-power applications, where the switching frequency is restricted to limit the power losses, the conventional tuning methods often fall short of achieving optimal performance and the stability of the system. This underscores the need for advanced approaches that can address these limitations and optimize the control gains more effectively. A detailed comparison is conducted between the conventional tuning and the proposed optimization method, in which the objective is to obtain an active power response that is decoupled from the the inner control loops dynamics while ensuring stability and exhibiting acceptable dynamic of the AC voltage loop. By leveraging the optimization algorithm, the control gains are adjusted to achieve this desired behavior, resulting in improved overall performance of the grid-forming-based system.**

***Index Terms*—Grid-forming Control, Optimal Gains Tuning, Small-Signal Stability, EMT Simulations**

I. Introduction

In transmission systems with high penetration rate of inverters-interfaced generation, the way to control the power inverters should be improved in order to overcome the limitations of the conventional grid-following control [1], [2]. In other words, the way to control power inverters has to be changed from "following the grid" to "supporting the grid". In this context, the grid-forming capability seems to be a suitable alternative for this aim thanks to the potential it brings to the power system e.g., voltage source behavior, inherent inertia emulation and the ability to operate in both grid-connected and standalone mode. Several grid-forming variants have been proposed in the literature. These solutions adopt more or less the idea of mimicking the swing equation of a synchronous machine (SM) [3], [4], [5], [6] to generate the control angle. Regarding the AC voltage magnitude, it is managed by a lower control level (i.e., inner control). One common solution to control the AC voltage magnitude is the cascaded control structure [7], [8], [9], [10]. This solution is favored for industrial applications because of the simplicity of its implementation and its ability to generate a current reference that serves to protect the inverter against faults. Yet, precise tuning of the controllers for the high power applications remains the major challenge with such a technique due to the limited switching frequency.

The overall control is typically tuned to achieve the desired dominant behavior, while the inner cascaded control is configured for a sufficiently fast response to avoid interactions with the power controllers. The bandwidth of the inner current control loop is restricted by the switching frequency, which in turn limits the bandwidth of the voltage control loop, thereby affecting the power control loops and the overall stability. Conventional tuning methods, although capable of ensuring stability, often fail to achieve decoupling between the power dynamics and inner control dynamics [7]. Numerous studies have addressed control design in high-power applications, where the switching frequency is below 5 kHz. A systematic approach to consider all dynamic states of the system and their potential interactions is the establishment of a small-signal state-space model for the tuning of multi-loop controllers in power converters [1], [7]. This approach facilitates comprehensive analysis and design of control strategies. Various techniques have been proposed in the literature, such as utilizing iterative methods based on pole placement in the complex plane using sensitivity parameters [7], or maximizing the damping factors while limiting the natural frequencies of eigenvalues [9], or by simply neglecting the AC voltage feed-forward in the inner current loop [11]. The aforementioned methods have demonstrated improvements over the conventional tuning for low-switching frequencies. However, it is worth noting that the methods in [7], [11] present an oscillatory response of the AC voltage and falls short in achieving decoupled behavior due to the slow response of the AC voltage, while the method proposed in [9] allows achieving a fast AC voltage response, however, it does not explicitly integrate decoupling conditions.

Submitted to the 23rd Power Systems Computation Conference (PSCC 2024).

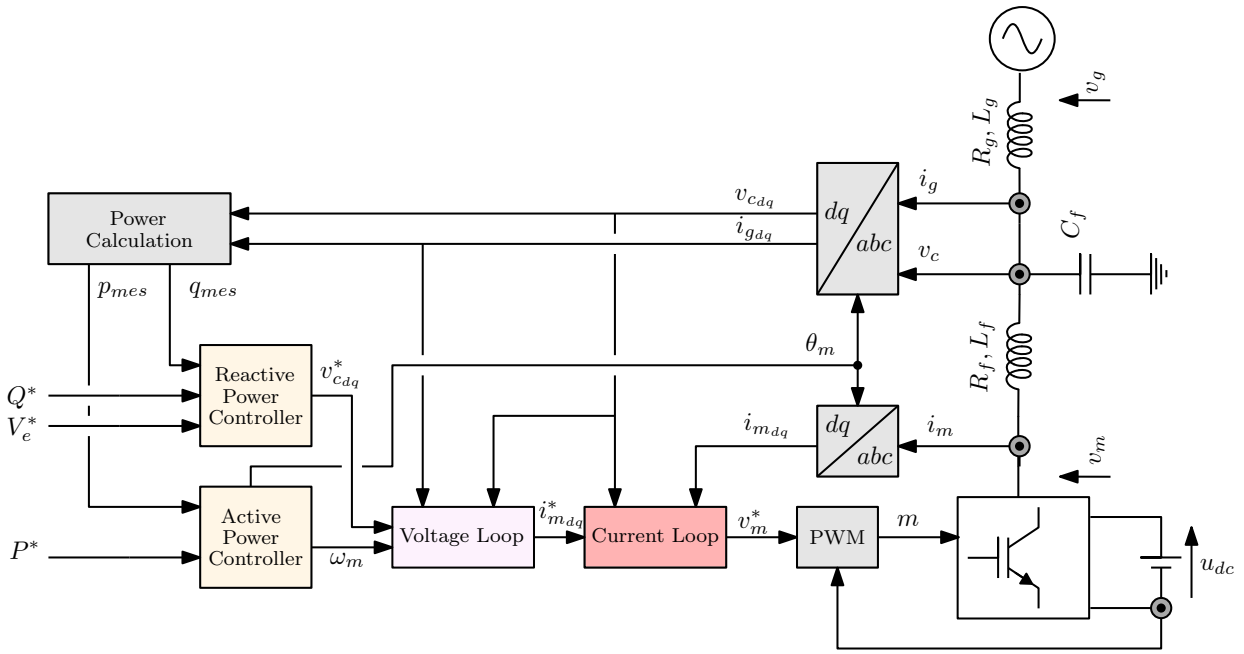

Fig. 1. Grid-Forming Control-based Two-Level VSC

To overcome the limitations of the conventional methods, This paper introduces an alternative iterative optimization method based on the time-domain response. The objective is to achieve a desired AC voltage response while maintaining the quasi-static response of the active power. A small-signal state-space model is derived, where the controllers' and feed-forward gains serve as the only remaining variables. By fulfilling the objective and the constraint, the active power and inner control loop dynamics are expected to be decoupled, resulting in an active power response resembling the quasi-static behavior, along with acceptable capacitor voltage dynamics.

The remaining of this paper is organized as follows. In section II, the grid-forming control is introduced and its model is provided. In section III, a small signal model of the grid-forming converter is derived and analyzed. Section IV proposes an optimal method to design the inner control gains. Finally, section V concludes the paper.

II. Grid-Forming Two-Level Voltage Source Converter

A. Plant Modelling

Fig. 1 presents a Two-level VSC connected to an equivalent AC grid via an LC filter. The equivalent AC grid is represented by an AC voltage source in series with its impedance R_g, L_g. The modeling of the plant in the Synchronous Rotating Frame (SFR) is given by (1)-(3). The state variables i_m, i_g and v_c are represented in the $d-q$ synchronous frame. i_m, i_g and v_c refer respectively to the converter current, the grid current and the converter voltage across the capacitor.

$$\frac{L_f}{\omega_b}\frac{di_{m_{dq}}}{dt} = v_{m_{dq}} - v_{c_{dq}} - R_f i_{m_{dq}} \pm \omega_g^* L_f i_{m_{qd}} \quad (1)$$

$$\frac{C_f}{\omega_b}\frac{dv_{c_{dq}}}{dt} = i_{m_{dq}} - i_{g_{dq}} \pm \omega_g^* C_f v_{c_{qd}} \quad (2)$$

$$\frac{L_g}{\omega_b}\frac{di_{g_{dq}}}{dt} = v_{c_{dq}} - v_{g_{dq}} - R_g i_{g_{dq}} \pm \omega_g^* L_g i_{g_{qd}} \quad (3)$$

L_f, L_g, C_f denote respectively the converter filter reactance, the grid reactance and the filter capacitor. ω_g^* and ω_b are the grid and the base frequencies, respectively. Along with the equations mentioned earlier, (4) and (5) provide the active power p_{vsc} and the reactive power q_{vsc} formulas.

$$p_{vsc} = v_{c_d} i_{g_d} + v_{c_q} i_{g_q} \quad (4)$$

$$q_{vsc} = v_{c_q} i_{g_d} - v_{c_d} i_{g_q} \quad (5)$$

The following sub-section will dive deeper into control structure, detailing the mathematical models of power and cascaded controls.

B. Grid-Forming Control

The adopted grid-forming control structure is illustrated in Fig. 1. It consists of a cascaded inner control loops to regulate the instantaneous AC voltage, and outer power control loops, which define the AC voltage setpoint. In the following sections, mathematical equations of each function are given.

1) Power Control Loop: The power controllers are in charge of regulating the active and reactive power, with separate loops for each, which are given by the Differential-algebraic equations (DAEs) in (6)-(10). The reactive power controller used in this work is a droop-based technique described by (9)-(10), while the active power loop is built adopting the Virtual Synchronous Machine concept in (6)-(8).

$$T_a\frac{d\Delta\omega_m}{dt} + k_d\left(\Delta\omega_m - \Delta\omega_g^*\right) = p^* - p_{vsc} \quad (6)$$

$$\frac{1}{\omega_b}\frac{d\delta_m}{dt} = \Delta\omega_m \tag{7}$$

$$\omega_m = \Delta\omega_m + \omega_g^* \tag{8}$$

$$\frac{dq_m}{dt} + \omega_f q_m = \omega_f q_{vsc} \tag{9}$$

$$v_{c_d}^* = |v|^* - m_q\left(q^* - q_m\right) \tag{10}$$

The VSC frequency and angle are represented by $\Delta\omega_m$ and δ_m, respectively, p^* serves as the reference power. The time constant of the rotational inertia is denoted as T_a. The damping factor is represented by k_d. Regarding the reactive power equations, q^*, q_m, m_q and ω_f denote the reactive power setpoint, the filtred measured reactive power, the droop gain and the cut-off frequency of the low-pass filter, respectively. $|v|^*$ is the reference value for the magnitude of the capacitor voltage.

2) Voltage Control Loop: The voltage loop aims to regulate the AC voltage at the filter capacitor level. It consists of dual PI controllers including the cross-coupling compensation terms $\omega_m v_{c_{dq}} C_f$, and the feed-forward terms $K_{FF_i} i_{g_{dq}}$:

$$\frac{d\xi_d}{dt} = k_{i_v}\left(v_{c_d}^* - v_{c_d}\right) \tag{11}$$

$$\frac{d\xi_q}{dt} = k_{i_v}\left(v_{c_q}^* - v_{c_q}\right) \tag{12}$$

$$i_{m_d}^* = K_{FF_i} i_{g_d} + k_{p_v}\left(v_{c_d}^* - v_{c_d}\right) - \omega_m C_f v_{c_q} + \xi_d \tag{13}$$

$$i_{m_q}^* = K_{FF_i} i_{g_q} + k_{p_v}\left(v_{c_q}^* - v_{c_q}\right) + \omega_m C_f v_{c_d} + \xi_q \tag{14}$$

$$v_{c_q}^* = 0 \tag{15}$$

The variables ζ_{dq}, k_{iv}, k_{pv} and K_{FF_i} in (11)-(14) denote respectively, the state variables of the voltage controllers integrators, the integral gain of the voltage PI controller, the proportional gain of the voltage PI controller and the grid current feed-forward gain.

3) Current Control Loop: Similarly to the voltage loop, the current loop aims to regulate the AC current at the filter reactance level, which serves for current limitation and protection in case of faults. The control loop consists of dual PI controllers including the cross-coupling compensation terms $\omega_m i_{c_{dq}} L_f$, and the feed-forward terms $K_{FF_v} v_{c_{dq}}$:

$$\frac{d\sigma_d}{dt} = k_{i_i}\left(i_{m_d}^* - i_{m_d}\right) \tag{16}$$

$$\frac{d\sigma_q}{dt} = k_{i_i}\left(i_{m_q}^* - i_{m_q}\right) \tag{17}$$

$$v_{m_d}^* = K_{FF_v} v_{c_d} + k_{p_i}\left(i_{m_d}^* - i_{m_d}\right) - \omega_m L_f i_{m_q} + \sigma_d \tag{18}$$

$$v_{m_q}^* = K_{FF_v} v_{c_q} + k_{p_i}\left(i_{m_q}^* - i_{m_q}\right) - \omega_m L_f i_{m_d} + \sigma_q \tag{19}$$

$$v_{m_d}^* = v_{m_d} \tag{20}$$

$$v_{m_q}^* = v_{m_q} \tag{21}$$

The variables σ_{dq}, k_{ii}, k_{pi} and K_{FF_v} in (16)-(19) denote respectively, the state variables of the current controllers integrators, the integral gain of the current PI controller, the proportional gain of the current PI controller and the capacitor voltage feed-forward gain.

III. Small Signal Model and Analysis

The plant and control equations combination (1)-(21) result in a system of 24 equations, out of which 13 are differential, and 11 are algebraic. The 24 equations can be written in the following state-space form:

$$\begin{cases} \dfrac{dx_{diff}}{dt} = f(x_{diff}, x_{alg}, u) \\ 0 = g(x_{diff}, x_{alg}, u) \\ y = h(x_{diff}, x_{alg}, u) \\ x_{diff} \in R^{N_{diff}}, x_{alg} \in R^{N_{alg}}, u \in R^p, y \in R^q \end{cases} \tag{22}$$

with $x_{alg} = [v_{m_{dq}}, p_{vsc}, q_{vsc}, \omega_m, v_{c_{dq}}^*, v_{c_{dq}}^*, i_{m_{dq}}^*]^T$, $x_{diff} = [v_{c_{dq}}, i_{m_{dq}}, i_{g_{dq}}, \Delta\omega_m, \delta_m, q_m, \zeta_{dq}, \sigma_{dq}]^T$ and $u = [p^*, q^*, v^*, v_{g_d}]^T$.

To study the system stability and dynamic behavior, a first step consists in linearizing the system, The linearization of the studied system must produce augmented matrices of minimal order 13. The calculation process for the augmented matrices is outlined as follows:

$$\begin{cases} A = \dfrac{\partial f}{\partial x_{diff}} - \dfrac{\partial f}{\partial x_{abg}} \times \dfrac{\partial g}{\partial x_{alg}}^{-1} \times \dfrac{\partial g}{\partial x_{diff}} \\ B = \dfrac{\partial f}{\partial u} - \dfrac{\partial f}{\partial x_{alg}} \times \dfrac{\partial g}{\partial x_{alg}}^{-1} \times \dfrac{\partial g}{\partial u} \\ C = \dfrac{\partial h}{\partial x_{diff}} - \dfrac{\partial h}{\partial x_{alg}} \times \dfrac{\partial g}{\partial x_{alg}}^{-1} \times \dfrac{\partial g}{\partial x_{diff}} \\ D = \dfrac{\partial h}{\partial u} - \dfrac{\partial h}{\partial x_{alg}} \times \dfrac{\partial g}{\partial x_{alg}}^{-1} \times \dfrac{\partial g}{\partial u} \end{cases} \tag{23}$$

$$\begin{cases} \dfrac{d\Delta x_{diff}}{dt} = A\Delta x_{diff} + B\Delta u \\ \Delta y = C\Delta x_{diff} + D\Delta u \end{cases} \tag{24}$$

To use properly the Jacobian method on DAE systems, it is necessary for the number of algebraic and differential variables to match the number of algebraic and differential equations, respectively. Additionally, the matrix $\frac{\partial g}{\partial x_{alg}}$ must not be singular [12].

A. Conventional Tuning [7]

With the assumption of an ideal decoupling of $d-$ and $q-$axes components, the current controller's open-loop transfer function can be written as:

$$h_{c,dq}(s) \approx \underbrace{\left(k_{pi} + \frac{k_{ii}}{s}\right)}_{\text{PI controler}} \cdot \underbrace{\frac{1}{1+T_v s}}_{\text{PWM approx}} \cdot \underbrace{\frac{1}{R_f(1+T_f s)}}_{\text{Filter reactance}} \tag{25}$$

$$T_f = \frac{L_f}{R_f \cdot \omega_b}, \qquad T_v \approx \frac{1}{2 \cdot f_{sw}} \tag{26}$$

T_v and T_f given in (26) are defined respectively as the time constant of the Pulse Width Modulation (PWM) approximation function and the time constant of the grid currents. The delay effect caused by the switching frequency f_{sw} of the converter PWM has been taken into account in order to properly tune the parameters of the inner current control loop. The PWM's

effect is approximated with a first-order transfer function as given in (25). The open-loop transfer function has no poles near or on the $jw - axis$. The current controller's PI tuning is done via the Modulus Optimum method (MO). MO method is a cancellation of the most dominant pole of the open-loop transfer function, and a gain selection with the purpose of achieving critical damping for the closed-loop transfer function. The controller's gains are given as in (27), where it is clearly demonstrated that both gains, and consequently the bandwidth, are limited by the switching frequency.

$$k_{p_i} = \frac{L_f}{2 \cdot \omega_b \cdot T_v}, \qquad k_{i_i} = \frac{R_f}{2 \cdot T_v} \tag{27}$$

The voltage control loop parameter tuning is constrained by the bandwidth of the current control loop. The closed-loop current controller can be expressed by a first-order transfer function for simplification. With the assumption of an ideal decoupling of the $d-$ and $q-$axes components, the voltage controller's open-loop transfer function can be written as:

$$h_{v,dq}(s) \approx \underbrace{\left(k_{pv} + \frac{k_{iv}}{s}\right)}_{\text{PI controller}} \cdot \underbrace{\frac{1}{1 + T_{eq,cc} \cdot s}}_{\text{current controller}} \cdot \underbrace{\frac{1}{T_{cc} \cdot s}}_{\text{filter capacitor}} \tag{28}$$

$$T_{eq,cc} \approx 2 \cdot T_v, \qquad T_{cc} = \frac{C_f}{\omega_b} \tag{29}$$

The open-loop transfer function has a pole near the $jw - axis$, consequently, the MO method is not the right one to use in this situation. The Symmetrical Optimum method (SO) is used for the voltage control loop. SO principle is based on obtaining the maximum phase margin at the open-loop transfer function's crossover frequency. PI gains are expressed as follows :

$$k_{p_v} = \frac{T_{cc}}{a \cdot T_{eq,cc}}, \quad k_{i_v} = \frac{T_{cc}}{a^3 \cdot T_{eq,cc}^2}, \quad a = 2\zeta + 1 \tag{30}$$

Usually, the voltage control bandwidth is chosen to be at most one-tenth of the current control bandwidth.

B. Validation of the Linearized Model

The verification of the linearized model is essential as the optimization approach introduced in this paper hinges on the time-domain outcomes derived from this linear representation. To affirm the model's validity, time-domain simulations have been performed in Fig. 2 and Fig. 3. The latter employ the conventional tuning gains and system parameters listed in Table I and II. The simulations illustrate the active power and capacitor voltage responses in response to a change of the active power and AC voltage references. The outcomes unveil the match between the linearized and nonlinear models.

C. Limitations of the Conventional Tuning

Tuning of both control loops' parameters relies heavily on the switching frequency of the converter, i.e. conventional tuning would give acceptable results in high switching frequency applications. However, for lower switching frequencies (i.e. high-power applications), the stability region reduces as well.

TABLE I
CONVENTIONAL INNER CONTROLLER' PARAMETERS

k_{p_v}	0.47 p.u	k_{i_v}	89.52 p.u
k_{p_i}	0.95 p.u	$k_{i_v i}$	9 p.u
K_{FF_v}	1	K_{FF_i}	0

TABLE II
SYSTEM AND POWER CONTROL PARAMETERS

L_f	0.1 p.u	L_g	0.1 p.u
R_f	0.003 p.u	R_g	0.003 p.u
V_m	1 p.u	V_g	1 p.u
C_f	0.2 p.u	T_a	2 s
k_d	3110 p.u	ω_f	$2\pi 10$ rad / s
ω_g^*	1 p.u	ω_b	$2\pi 50$ rad / s
m_q	0 p.u		
f_{sw}	3 KHz		

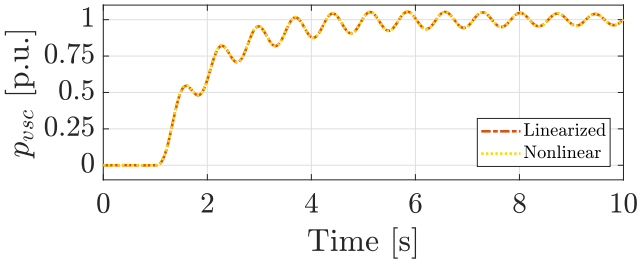

Fig. 2. Active Power Response to $\Delta p^* = 1\ p.u.$

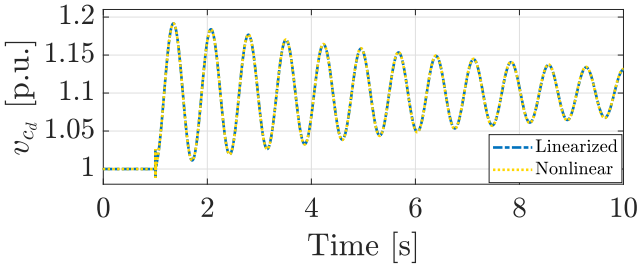

Fig. 3. Capacitor Voltage Response to $\Delta|v|^* = 0.1\ p.u.$

With smaller stability regions, more problems are encountered, since even if stability is ensured, the dynamics might be affected negatively due to close control loops bandwidths as demonstrated in [2], [9] and as shown in Fig. 2 and Fig. 3.

D. Prior alternative Control tuning Methods

Various algorithms based on the pole placement method have been proposed in the literature to overcome the limitations of the conventional tuning [2], [9], [7], [10], [11]. The method in [2], [7] determines the eigenvalues for a wide range of controller gains and selects the one with the highest damping factor. In [7], the authors have studied the parameters sensitivity and their impact on the eigenvalues evolution in order to move the pole further in stable plan. In

[10], [11], the authors have highlighted the significant effect of the feed-forward terms on the stability of the AC voltage i.e., referring to [11], the system dynamics can been significantly improved by neglecting the voltage feed-forward term in the current control loop, and by using the controller gains based on the conventional tuning. Although prior methods show improvements over the conventional tuning for low-frequency applications, the decoupling aspect between inner and outer controls has not been considered, resulting in control interactions between the power loops and the AC voltage loop.

IV. Algorithm Proposed for Control Parameter Tuning

The main objective of the proposed algorithm is to achieve a stable system with a desired behavior. To accomplish this objective, the gains k_{pv}, k_{pi}, k_{iv}, k_{ii}, K_{FFv}, and K_{FFi} are optimized. The optimization process aims to closely match the behavior of an desired objective function, while respecting some imposed constraints. The algorithm specifically focuses on the time-domain responses of capacitor voltage and the active power, with the capacitor voltage response as the objective function and active power response as the constraint.

Various works such as [2], have proposed a quasi-static model for active power. This model describes the transfer function of the dominant active power behavior, considering only the dominant poles and disregarding faster dynamics that may arise from different state variable dynamics. Consequently, the quasi-static active power model is employed as a constraint function in this optimization. The goal is to decouple the active power behavior from the capacitor voltage dynamics. Therefore, the optimization algorithm imposes sufficiently fast capacitor voltage dynamics, which being restricted the converter bandwidth. The inclusion of K_{FF_v} and K_{FF_i} in the control loops is motivated by the optimization purposes, i.e., it has been found that eliminating the feed-forward grid voltage enhances the stability of responses with different Short Circuit Ratio configurations, as suggested in [10], [11]. By incorporating K_{FF_v} and K_{FF_i} as part of the optimized parameters, the algorithm gains additional degrees of freedom, leading to the potential for better outcomes.

In order to describe the procedure, it is essential to define the desired behavior of the capacitor voltage and the power constraint.

A. The desired voltage response

To avoid interactions between capacitor voltage dynamics and power dynamics, it is crucial to achieve a rapid voltage behavior. To accomplish this, a first-order voltage dynamics with a targeted time constant of T_{des} = 50ms is chosen as the desired voltage behavior for the optimization. The desired voltage transfer function is expressed as:

$$\Delta v_{c_d}^{des} = \frac{1}{1 + T_{des} \cdot s} \Delta v_{c_d}^{*} \tag{31}$$

B. The Quasi-static power response

The quasi-static active power response is given by the equation below:

$$\Delta p_{vsc}^{des} = \frac{1}{1 + \frac{k_d}{K_c \omega_b} s + \frac{T_a}{K_c \omega_b} s^2} \Delta p^{*} \tag{32}$$

where K_c referred to the synchronizing torque equal to $K_c = V_m V_g / X_g$. Both the grid and converter's voltage amplitudes, denoted by V_m and V_g respectively.

C. Procedure of Optimization

The objective of the optimization process is to achieve a fast response of the capacitor voltage v_c while preserving the quasi-static behavior of the active power p_{vsc}. The output variables v_c and p_{vsc} from the linearized model in (24) are used as inputs for optimization function. To accomplish the aforementioned objective, the desired behaviors for both the capacitor voltage response and the quasi-static response of the active power are taken into consideration. Based on these desired responses, an objective function and a non-linear constraint are formulated. Instead of traditional pole placement, a curve-fitting approach is utilized to minimize error and ensure that the system behaves as closely as possible to the desired response, while still adhering to the constraint.

1) **The objective function:** The objective function is described as follows:

$$F_{obj} = \left|\left| v_{c_d}(kT) - v_{c_d}^{des}(kT) \right|\right|_2 \tag{33}$$

T stands for a sampling time (for this work $T = 100\mu$s), and the time range must also be defined to optimize for this particular range.

2) **The constraint function:** The constraint function focuses on the active power behavior and is described as follows:

$$F_{const} = \left|\left| P_{vsc}(kT) - p_{vsc}^{des}(kT) \right|\right|_2 \tag{34}$$

Using curve fitting rather than pole placement, results in an automatic placement of poles that achieves a close match to the desired behavior. The algorithm, outlined in (35) utilizes a vector of optimized parameters (gains) denoted by x. Additionally, lower and upper bounds, lb and ub, are employed to restrict the controller's bandwidth. lb has been set to zero while ub is defined from the conventional tuning method. The coefficient m in (35) defines the tolerated norm error and the accuracy of the algorithm in respecting the constraint i.e., smaller m results in a high accuracy between the dynamic active power and the desired quasi-static active power. In this paper the tolerated norm error is set to m = 0.2.

$$\min_x F_{obj}(x) \text{ such that } \begin{cases} F_{const}(x) \leq m \\ lb \leq x \leq ub \end{cases} \tag{35}$$

$$x = [k_{p_v},\ k_{p_i},\ k_{i_v},\ k_{i_i},\ K_{FF_v},\ K_{FF_i}]$$

TABLE III
CASCADED PI CONTROLLER' PARAMETERS

Gains	Conventional	Method in [7]	Method in [11]	Method in [9]	Proposed
k_{p_v}	0.47 p.u	1.795 p.u	0.47 p.u	0.52 p.u	0.89 p.u
k_{i_v}	89.52 p.u	80.79 p.u	89.52 p.u	1.16 p.u	47.01 p.u
k_{p_i}	0.95 p.u	0.63 p.u	0.95 p.u	0.73 p.u	0.89 p.u
k_{i_i}	9 p.u	20 p.u	9 p.u	1.19 p.u	7.54 p.u
k_{ff_v}	1 p.u	1 p.u	0 p.u	1 p.u	0.99 p.u
k_{ff_i}	0 p.u	0 p.u	0 p.u	1 p.u	0.94 p.u

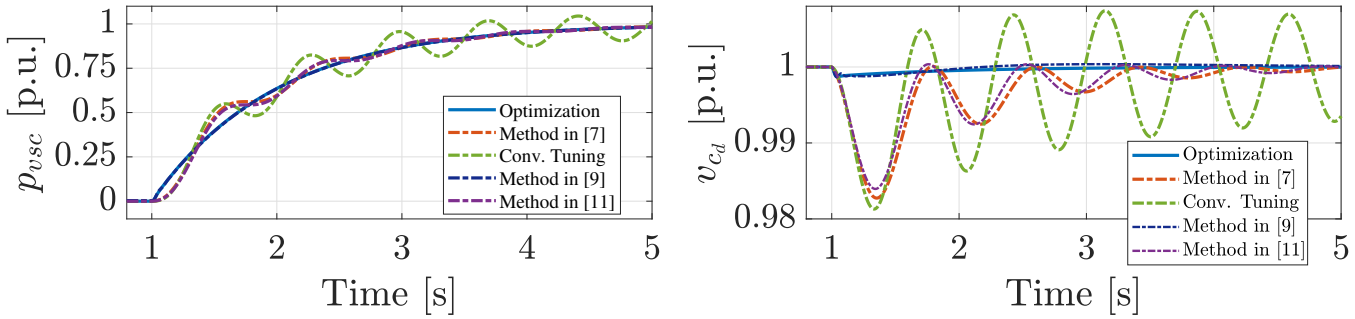

Fig. 4. Active Power change of $p^* = 1$ p.u

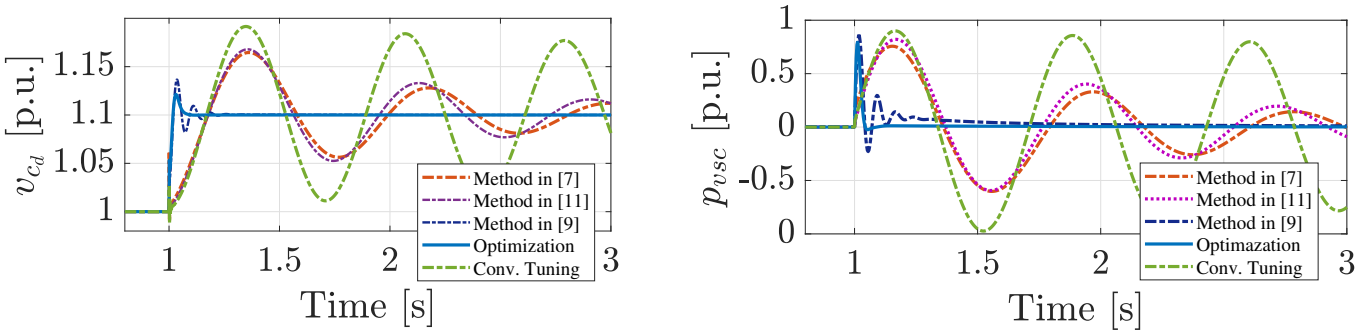

Fig. 5. Capacitor Voltage change of $|\Delta v|^* = +10\%$

V. SIMULATION AND RESULTS

In this section, time-domain responses are recorded for both p_{vsc} and v_{c_d} to observe how the system performs under the constraint function imposed on the active power while aiming to achieve the desired behavior of the capacitor voltage. Two different scenarios are considered in this analysis to assess the system response to both power reference change and voltage reference change. The system response is shown for four sets of gains listed in Table III: gains obtained through the proposed algorithm, through conventional tuning, through the algorithm detailed in [7], and finally, through the the solution proposed in [11]. Time-domain simulation results and dynamic behaviors are recorded for two test cases:

- Δp^* change of 1 p.u at t=1 s shown in Fig. 4.
- $\Delta |v|^*$ change of 0.1 p.u at t=1 s shown in Fig. 5.

One can notice form the obtained results that with the conventional tuning parameters and those from [7], [11], the active power response, although stable, displays significant oscillations. This indicates that the power behavior is not effectively decoupled from the capacitor voltage response, which is confirmed by the capacitor voltage response.

Comparing the optimized control gains to those obtained by the method in [9], it can be observed that with both methods the power response obtained for a power reference change aligns closely the quasi-static active power response, resulting in satisfactory outcomes. The capacitor voltage based on the proposed optimal method reaches a steady state at the time specified by the objective function i.e, 50ms. Again, the obtained voltage response based on the proposed method is still closer to the one obtained using the method in [9]. Although the obtained results look almost similar to those obtained using the gains from [9], the tuning methods are different. Additionally, the proposed method includes the decoupling between the inner and the outer loops as a constraint for the tuning, while in [9], the control layers decoupling has not been

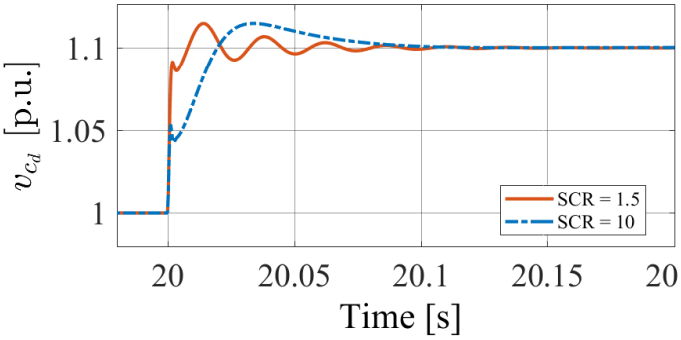

Fig. 6. Capacitor Voltage Response to $\Delta|v|^* = 0.1\ p.u.$

explicitly studied and considered.

To evaluate the stiffness of grid-forming converter based on the proposed tuning, a simulation result has been presented in Fig. 6, considering very weak grid AC system (Short Circuit Ratio of SCR = 1.5). One can notice the that system is stable for AC voltage change with an operating point of 1 p.u.

VI. Conclusion

This work has proposed an optimization method for the inner grid-forming controllers. The goal was to produce a set of parameters that would result in a stable and decoupled dynamics with satisfactory behavior. A small-signal model has been derived to be used for the optimization purpose. The latter has involved defining an objective and constraints to achieve decoupled behavior while closely approximating the quasi-static active power model's response in the time-domain. To demonstrate the effectiveness of this method, a comparison was conducted with conventional tuning methods. The obtained results have shown significant improvements, where the power response was decoupled from the faster voltage loop dynamics, allowing the latter to reach a predetermined short rise time.

References

[1] "High Penetration of Power Electronic Interfaced Power Sources (HPoPEIPS)," ENTSO-E, Technical, Mar. 2017. [Online]. Available: https://consultations.entsoe.eu/system-development/entso-e-connection-codes-implementation-guidance-d-3

[2] T. QORIA, "Grid-forming control to achieve a 100% power electronics interfaced power transmission systems," ENSAM, Paris, 2020.

[3] S. D'Arco and J. A. Suul, "Equivalence of Virtual Synchronous Machines and Frequency-Droops for Converter-Based MicroGrids," IEEE Trans. Smart Grid, vol. 5, no. 1, pp. 394–395, Jan. 2014, doi: 10.1109/TSG.2013.2288000.

[4] T. QORIA, F. GRUSON, F. COLAS, G. Denis, T. PREVOST, and G. Xavier, "Inertia effect and load sharing capability of grid forming converters connected to a transmission grid," The 15th IET international conference on AC and DC Power Transmission, UK, p. 6, Jan. 2019.

[5] M. Ashabani, F. D. Freijedo, S. Golestan, and J. M. Guerrero, "Inducverters: PLL-Less Converters With Auto-Synchronization and Emulated Inertia Capability," IEEE Trans. Smart Grid, vol. 7, no. 3, pp. 1660–1674, May 2016, doi: 10.1109/TSG.2015.2468600.

[6] T. Qoria, E. Rokrok, A. Bruyere, B. Francois, and X. Guillaud, "A PLL-Free Grid-Forming Control With Decoupled Functionalities for High-Power Transmission System Applications," IEEE Access, vol. 8, pp. 197363–197378, 2020, doi: 10.1109/ACCESS.2020.3034149.

[7] S. D'Arco, J. A. Suul, and O. B. Fosso, "Automatic Tuning of Cascaded Controllers for Power Converters Using Eigenvalue Parametric Sensitivities," IEEE Trans. Ind. Appl., vol. 51, no. 2, pp. 1743–1753, Mar. 2015, doi: 10.1109/TIA.2014.2354732.

[8] Z. Li, C. Zang, P. Zeng, H. Yu, S. Li, and J. Bian, "Control of a Grid-Forming Inverter Based on Sliding-Mode and Mixed H_2/H_∞ Control," IEEE Trans. Ind. Electron., vol. 64, no. 5, pp. 3862–3872, May 2017, doi: 10.1109/TIE.2016.2636798.

[9] T. Qoria, F. Gruson, F. Colas, X. Guillaud, M. Debry, and T. Prevost, "Tuning of Cascaded Controllers for Robust Grid-Forming Voltage Source Converter," in 2018 Power Systems Computation Conference (PSCC), Jun. 2018, pp. 1–7. doi: 10.23919/PSCC.2018.8443018.

[10] M. H. Ravanji, D. B. Rathnayake, M. Z. Mansour and B. Bahrani, "Impact of Voltage-Loop Feedforward Terms on the Stability of Grid-Forming Inverters and Remedial Actions," in IEEE Transactions on Energy Conversion, vol. 38, no. 3, pp. 1554-1565, Sept. 2023, doi: 10.1109/TEC.2023.3246566.

[11] G. Denis, T. Prevost, P. Panciatici, X. Kestelyn, F. Colas and X. Guillaud, "Improving robustness against grid stiffness, with internal control of an AC voltage-controlled VSC," 2016 IEEE Power and Energy Society General Meeting (PESGM), Boston, MA, USA, 2016, pp. 1-5, doi: 10.1109/PESGM.2016.7741341.

[12] Q. Cossart, F. Colas, and X. Kestelyn, "A Novel Event- and Non-Projection-Based Approximation Technique by State Residualization for the Model Order Reduction of Power Systems with a High Renewable Energies Penetration," IEEE Trans. Power Syst., pp. 1–1, 2020, doi: 10.1109/TPWRS.2020.3010891.